Magnetic tunnel junctions based on CrO_2/SnO_2 epitaxial bilayers

G. X. Miao, P. LeClair,[a] and A. Gupta
Center for Materials for Information Technology, University of Alabama, Tuscaloosa, Alabama 35487

G. Xiao
Department of Physics, Brown University, Providence, Rhode Island 02912

M. Varela and S. Pennycook
Oak Ridge National Laboratory, Oak Ridge, Tennessee 37831

(Received 18 November 2005; accepted 11 May 2006; published online 14 July 2006)

Magnetic tunnel junctions were fabricated using thin films of the half-metallic ferromagnet CrO_2, employing SnO_2 tunnel barriers. Heteroepitaxial CrO_2/SnO_2 bilayers were grown on (100)-TiO_2 substrates via chemical vapor deposition. X-ray diffraction and transmission electron microscopy confirmed heteroepitaxy. A polycrystalline cobalt film forms the top magnetic electrode, yielding $CrO_2(001)/SnO_2(001)/Co$ structures after patterning. Tunneling magnetoresistances (TMR) up to +14% at 10 K were observed. The sign of the TMR reverses for barrier thicknesses <1 nm, attributed to tunneling being dominated by Co-3*d* states at low thicknesses and Co-4*s* states at larger thicknesses. © *2006 American Institute of Physics*. [DOI: 10.1063/1.2216109]

Since the initial observations of substantial room-temperature magnetoresistance in magnetic tunnel junctions about a decade ago,[1,2] there has been a surge of interest in spin polarized tunneling. This is due in a large part to the practical significance for improved magnetoresistive devices for next generation magnetic sensors and memory cells. A simple model for spin polarized tunneling was provided by Julliére[3] in 1975 based on the work of Meservey and Tedrow,[4] soon after the initial concept was proposed. The Julliére model relates the tunneling spin polarization (P) of the two ferromagnetic electrodes and the expected magnitude of the tunneling magnetoresistance (TMR) effect via the simple relationship $\mathrm{TMR}=2P_1P_2/(1-P_1P_2)$. Though the effective P is strongly dependent on, e.g., ferromagnet-insulator bonding and the symmetry of the Bloch states involved in tunneling,[5–8] the Julliére model has been quite successful in accounting for the magnitude of the TMR for tunnel junctions utilizing amorphous AlO_x barriers. These materials have effective $P\sim 50\%$,[9] and consistent with the predictions of the Julliére model, the maximum observed TMR in AlO_x-based devices has been $\sim 60\%-70\%$ at room temperature.[10] One approach to enhancing the TMR would be to use electrode materials with higher P, in particular, half-metallic ferromagnets with $P\sim 100\%$. Though dozens of systems have been predicted to be half-metallic, CrO_2 is essentially the only material that has been experimentally shown to definitively be a half-metal.[11]

Despite this unique characteristic, there has been limited work reported thus far on CrO_2-based devices primarily because of the difficulties related to thin film synthesis of this metastable phase. TMR of −8% was observed in CrO_2/Co structures at 4.2 K, using the naturally formed Cr_2O_3 on the surface of CrO_2 as a tunnel barrier.[12] Negative TMR means the resistance change, i.e., the resistance of the junction with parallel alignment of the magnetic electrodes is higher than with antiparallel alignment. This is in contrast to conventional magnetic tunnel junctions with AlO_x barriers.[9] Since CrO_2 is half-metallic with $P>0$, this implies (within the Julliére model) $P<0$ for Co with Cr_2O_3 tunnel barriers, similar to earlier results for $Co/SrTiO_3$ reported by de Teresa *et al.*[5] Interestingly, an inverse TMR has also been reported for CrO_2/Co tunnel junctions consisting of a Cr_2O_3/AlO_x double barrier,[13] even with a relatively thick AlO_x layer. In this case, however, $P>0$ is expected for both CrO_2 and Co/Al_2O_3, and the origin of the negative TMR is ambiguous. In this letter, we report large positive TMR values in $CrO_2/SnO_2/Co$ structures.

Band structure calculations suggest that heterostructures of CrO_2 with metallic or semiconducting rutile oxide spacer layers can possibly exhibit very high magnetoresistance.[14] However, difficulties related to the growth of the ferromagnetic and spacer materials under compatible conditions have hampered experimental progress, and it is only recently that the fabrication of CrO_2/RuO_2 heterostructures has been realized using chemical vapor deposition (CVD).[15] In this letter, we report results on magnetic tunnel junctions fabricated using heteroepitaxial thin films of CrO_2/SnO_2 grown by CVD on rutile titanium dioxide (TiO_2) substrates.[16] SnO_2 is a semiconductor with the same rutile structure as CrO_2 and is widely used as a sensor material. The surface electrical properties of SnO_2 are sensitive to adsorbed gases, which can change the number of electrical carriers,[17] possibly leading to multifunctional devices. The transport properties of SnO_2 are also very sensitive to small differences in the oxygen stoichiometry, making the CrO_2/SnO_2 system an interesting one in which to study the interplay of spin-dependent and defect-mediated transport. A polycrystalline cobalt film is used as the second ferromagnetic electrode. We have observed positive TMR values as high as 14% in these junctions at 10 K. Additionally, we have found an intriguing dependence of TMR on SnO_2 barrier thickness, attributed to a crossover from tunneling dominated by *d*-like states at low thicknesses to tunneling dominated *s*-like states at large barrier thicknesses.

The CrO_2/SnO_2 heterostructures are grown on (100)-oriented TiO_2 substrates under atmospheric conditions by CVD in a 1 in. diameter quartz tube reactor placed inside a two-zone furnace. The precursor materials are loaded inside a small quartz boat in the source zone, while the substrates are placed in the higher temperature reaction zone. The CrO_2

[a]Electronic mail: pleclair@alum.mit.edu

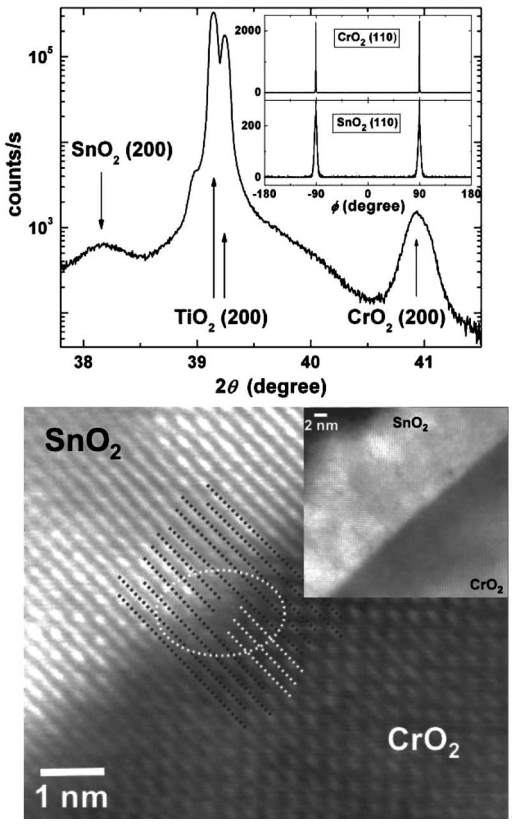

FIG. 1. Upper: θ-2θ XRD scan for a TiO_2 substrate/100 nm CrO_2/100 nm SnO_2 heterostructure. The inset shows the off-axis scans for the (110) peaks of both layers. The values of the angle are 43.4° and 44.1° for CrO_2 and SnO_2, respectively. Lower: high resolution cross-section STEM image of the CrO_2/SnO_2 interface (no Cr_2O_3 natural barrier is observed). An edge dislocation core resulting from the lattice mismatch is highlighted. The inset shows a lower magnification image.

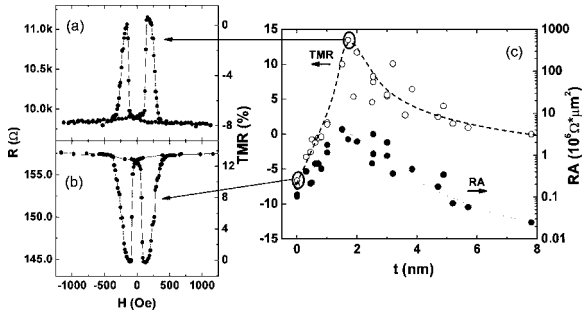

FIG. 2. (a) Resistance vs field for junctions with (a) a 1.7 nm SnO_2 barrier and (b) a natural barrier, exhibiting positive and negative TMRs, respectively. (c) Plot of the TMR and resistance-area product (*RA*) for $CrO_2/SnO_2/Co$ junctions with varying SnO_2 barrier thickness. The lines are a guide to the eye. All the measurements are at 10 K with 1 mV bias voltage.

and SnO_2 films are deposited sequentially using CrO_3 and SnI_4 precursors, respectively, with oxygen as a carrier gas. We maintain the source and substrate temperatures for the two deposition runs at 260 °C/400 °C and 80 °C/350 °C, respectively. While both the films can be grown under compatible conditions, it is still necessary to stop the growth after each layer to exchange the precursors and grow the next layer. This is due to the fact that both the CrO_2 and SnO_2 precursors are solids at room temperature, and there is no convenient *in situ* scheme for switching from one to the other during the deposition process. Electron microscopy observations were carried out in an aberration corrected scanning transmission electron microsope (STEM) (VG Microscopes HB501UX) operated at 100 kV. Specimens for STEM were preprared by conventional methods, grinding, dimpling, and Ar ion milling.

After growth of the CrO_2/SnO_2 heterostructures, standard optical lithography and lift-off processes were employed to coat the samples with a 100 nm thick SiO_2 dielectric layer, leaving windows of different dimensions. This process requires exposure of the SnO_2 to air, precluding a study of the effect of O_2 pressure during SnO_2 growth. A 50 nm thick layer of Co was then deposited using dc magnetron sputtering to form the top electrode.[11] In the final step, a 50 nm layer of Ti is deposited for the top contact. All the junctions are aligned along the (001) direction, which is the in-plane easy-axis magnetization direction for the CrO_2 film. We have measured the dc magnetoresistance using a standard four-probe method, ensuring that all the contact resistance values are less than 10 Ω to eliminate current crowding.[18] We will limit our discussions in this letter to the results obtained on 35×7 μm^2 CrO_2–Co junctions, where the measured voltage is referred to with respect to the CrO_2 electrode, i.e., for $V>0$ electrons tunnel from Co to CrO_2.

Figure 1 shows the normal θ-2θ scan around the (200) peaks of the film and the substrate. The (200) rocking curve full width at half maximum of the CrO_2 layer is 0.16°, compared to 2.3° for the SnO_2 layer, indicating higher quality of CrO_2 compared to SnO_2. Nevertheless, the two layers are heteroepitaxial, as is confirmed from the twofold symmetry of the off-axis (110) peaks shown in the inset. Further confirmation of the heteroepitaxy has been obtained from investigations of the films using transmission electron microscopy. Figure 1 also shows a high resolution cross-sectional *Z*-contrast image of the interface region for a 50 nm CrO_2/20 nm SnO_2 heterostructure on a (100)-TiO_2 substrate. The two layers are well aligned and form an abrupt interface, with no evidence of an interfacial layer of Cr_2O_3, overall indicating that the SnO_2 layer is indeed highly crystalline and uniform. This is similar to what we have reported for CrO_2/RuO_2 structures, where subsequent RuO_2 deposition removed the existing natural barrier on as-deposited CrO_2 films.[15] Due to the large lattice mismatch between the two oxides in both in-plane directions (~9%), dislocations can be observed at the interface along with other defects, such as step disorders. A dislocation is highlighted in Fig. 1, where an extra atomic plane can be seen on the CrO_2 side. Closer analysis of the images indicates that the interface width along the growth direction is around 1 nm (perpendicular to the image plane), indicating a small degree of either interface roughness or intermixing.

Figure 2(a) shows the field dependence of the tunneling resistance (R) and the TMR ($\Delta R/R_p$) at 10 K for a 100 nm CrO_2/1.7 nm SnO_2/50 nm Co structure. Here, R is measured at close to zero bias and R_p is the measured resistance in the parallel orientation. The observed changes in R are associated with the moment reversals of the two magnetic electrodes and the switching fields for these changes correspond closely with the respective coercivities. The lower and higher field values correspond to switching of the Co and CrO_2 layers, respectively. For comparison, we also show in Fig. 2(b) the TMR of a CrO_2/Cr_2O_3 (natural barrier)/Co junction at 10 K that was similarly processed. It is interesting to note that while the natural barrier junction in Fig. 2(b) exhibits an inverse TMR (−8%), the $CrO_2/SnO_2/Co$ junc-

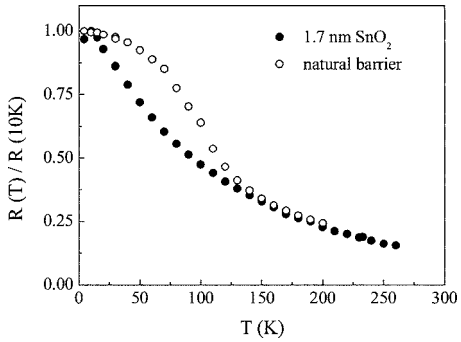

FIG. 3. Resistance vs temperature for a junction with a 1.7 nm SnO_2 barrier (closed) and a natural barrier (open).

tion in Fig. 2(a) displays normal TMR (+14% in this case).

We have studied the magnetoresistive properties of the $CrO_2/SnO_2/Co$ structures as a function of the SnO_2 barrier thickness t, and the results are shown in Fig. 2(c). The data point corresponding to zero SnO_2 thickness is for a junction consisting of only the natural Cr_2O_3 barrier that exhibits an inverse MR, as seen in Fig. 2(b). With increasing SnO_2 layer thickness, the TMR initially decreases in magnitude, and eventually changes sign. The TMR shows a peak value for a nominal SnO_2 barrier thickness of 2 nm. The TMR remains positive thereafter, but shows a decrease with further increase in the barrier thickness. Thus in this system it is clear that the amplitude of the spin polarization and even its sign depend on the barrier material. Though the effective spin polarization for Co/SnO_2 is unknown, if we assume a conservative value of 35%, the maximum TMR value observed gives $P_{CrO_2} \approx 19\%$. This is significantly lower than the expected $P = 100\%$, probably a result of inelastic tunneling due to slight SnO_2 structural disorder, as discussed below.

The transport behavior of magnetic tunnel junctions is well known to be strongly influenced by the electronic structure of the barrier and barrier-electrode interface.[5–9] Due to its half-metallic nature, in principle, CrO_2 will maintain positive spin polarization in all cases. For Co, however, it is known that at the Fermi level, the spin polarization is positive for *s*-like electrons and negative for *d*-like electrons.[8,19] Depending on the nature of the Co-insulator interface bonding[5] and the complex band structure of the insulator,[6,7] either *s*-like or *d*-like states may dominate the tunneling current. In the present case, both natural and SnO_2 barriers in contact with Co must be considered. For natural barriers alone (at low SnO_2 thicknesses where coverage is incomplete a natural barrier will be present), the CrO_2-natural barrier interface plays a dominant role, while for larger thicknesses we expect that the CrO_2-SnO_2 interface is dominant. Therefore, we attribute the observed TMR reversal with increasing SnO_2 thickness to the change in bonding at the Co/oxide interface, from predominantly $Co-Cr_2O_3$ to predominantly $Co-SnO_2$. In our view, at low SnO_2 thicknesses where the Co/Cr_2O_3 interface plays the major role, tunneling is dominated by negatively polarized *d*-like electrons due to predominantly $sd\sigma$ bonding. For increasing SnO_2 thickness, $ss\sigma$ bonding at the Co/SnO_2 interface favoring positively polarized *s*-like electrons dominates. The negative TMR of de Teresa *et al.* was attributed to altered ferromagnet-insulator bonding,[5] as was a reduction of the TMR for ultrathin AlO_x barriers.[20]

We have also observed that the resistance-area product as a function of SnO_2 thickness displays a nonmonotonic behavior, as shown in Fig. 2(c) (note the logarithmic *RA* scale). Interestingly, *RA* increases rapidly from 0 to 2 nm, and then decreases gradually. For ideal elastic tunneling, $RA \sim \exp(t)$, and the *RA* product should increase linearly with thickness on a semilog scale, and this is roughly the case for $t < 2$ nm. The decrease in *RA* beyond ~2 nm, however, is inconsistent with purely tunneling transport (either elastic or inelastic). One possible explanation for the decreased *RA* product at larger SnO_2 thicknesses is increasing structural disorder, not unexpected given a lattice mismatch of ~9%. If the concentration of defect states increases with thickness, at some point it becomes sufficient to form an impurity band near E_F. In this case, the conduction mechanism will gradually change from purely tunneling regime to a more metallic one, strongly decreasing the resistance. In this case, one also expects a strong temperature dependence of the tunneling resistance. Figure 3 shows resistance versus temperature for a junction with a 1.7 nm SnO_2 barrier and a natural barrier. Both the SnO_2 and natural barrier junctions show a significant decrease of resistance as temperature increases, consistent with defect-assisted tunneling. A detailed analysis of the temperature and bias dependence of the magnetoresistance in this system will be the subject of a subsequent paper.

This research was supported by NSF MRSEC Grant No. DMR-0213985 and NSF Grant No. DMR-0520491. Research at ORNL was sponsored by the Laboratory Directed Research and Development Program of ORNL, managed by UT-Batelle, LLC, for the U.S. Department of Energy under Contract No. DE-AC05-00OR22725.

[1] J. S. Moodera, L. R. Kinder, T. M. Wong, and R. Meservey, Phys. Rev. Lett. **74**, 3273 (1995).
[2] T. Miyazaki and N. Tezuka, J. Magn. Magn. Mater. **139**, 231 (1995).
[3] M. Julliére, Phys. Lett. **54A**, 225 (1975).
[4] R. Meservey and P. M. Tedrow, Phys. Rep. **238**, 173 (1994).
[5] J. M. de Teresa, A. Berthelemy, A. Fert, J. P. Contour, F. Montaigne, and P. Seneor, Science **286**, 507 (1999).
[6] J. M. MacLaren, X. G. Zhang, W. H. Butler, and X. Wang, Phys. Rev. B **59**, 5470 (1999).
[7] W. H. Butler, X. G. Zhang, T. C. Shulthess, and J. M. MacLaren, Phys. Rev. B **63**, 054416 (2001).
[8] E. Y. Tsymbal and D. G. Pettifor, J. Phys.: Condens. Matter **9**, L411 (1997).
[9] P. LeClair, H. J. M. Swagten, and J. S. Moodera, in *Ultrathin Magnetic Structures III: Fundamentals of Nanomagnetism*, edited by J. A. C. Bland and B. Heinrich (Springer, Berlin, 2005), p. 51.
[10] D. Wang, C. Nordman, J. M. Daughton, Z. Qian, and J. Fink, IEEE Trans. Magn. **40**, 2269 (2004).
[11] A. Anguelouch, A. Gupta, G. Xiao, D. W. Abraham, Y. Ji, S. Ingvarsson, and C. L. Chien, Phys. Rev. B **64**, 180408(R) (2001).
[12] A. Gupta, X. Y. Li, and G. Xiao, Appl. Phys. Lett. **78**, 1894 (2001).
[13] J. S. Parker, P. G. Ivanov, D. M. Lind, P. Xiong, and Y. Xin, Phys. Rev. B **69**, 220413 (2004).
[14] A. M. Bratkovsky, Appl. Phys. Lett. **72**, 2334 (1998).
[15] G. X. Miao, A. Gupta, H. Sims, W. H. Butler, S. Ghosh, and G. Xiao, J. Appl. Phys. **97**, 10C924 (2005).
[16] A. Gupta, X. W. Li, S. Guha, and G. Xiao, Appl. Phys. Lett. **75**, 2996 (1999).
[17] C. Kilic and A. Zunger, Phys. Rev. Lett. **88**, 095501 (2002).
[18] J. S. Moodera, L. R. Kinder, J. Nowak, P. LeClair, and R. Meservey, Appl. Phys. Lett. **69**, 708 (1996).
[19] J. A. Hertz and K. Aoi, Phys. Rev. B **8**, 3252 (1973).
[20] M. Munzenberg and J. S. Moodera, Phys. Rev. B **70**, 060402(R) (2004).